

A Refined Understanding of the Ice Cloud Longwave Scattering Effects in Climate Model

Chongxing Fan¹, Yi-Hsuan Chen², Xiuhong Chen¹, Wuyin Lin³, Ping Yang⁴, and Xianglei Huang¹

¹University of Michigan

²Princeton University

³Brookhaven National Laboratory

⁴Texas A&M University

September 16, 2023

Abstract

Because longwave (LW) absorption by greenhouse gases and clouds is more significant than the LW scattering effect by clouds, most climate models neglect cloud LW scattering to save computational costs. Ignoring cloud LW scattering directly overestimates outgoing longwave radiation (OLR). This study included ice-cloud LW scattering treatment in the Exascale Energy Earth System Model (E3SM) version 2 and ran fully-coupled simulations, prescribed sea surface temperature simulations, and offline radiative transfer calculations to comprehensively assess the impact of ice-cloud LW scattering on global climate simulation. The instantaneous effect due to ice-cloud LW scattering reduces the OLR by ~ 1 W/m² on the global average and 2 W/m² on the tropical average. Tropospheric warming and high cloud amount reduction act to partially compensate for such instantaneous OLR reduction caused by the inclusion of LW scattering. When the simulation reaches the equilibrium, the surface warms by 0.66 K on average with respect to the simulation without LW scattering, with the Arctic surface temperature differences more than twice as large as that of the global mean. The impact of including LW scattering on the simulated climate change in response to 4×CO₂ is also assessed. While including the cloud LW scattering does not significantly modify radiative forcing and total radiative feedback under such a scenario, it results in a 10% more positive cloud feedback.

26 **Abstract**

27 Because longwave (LW) absorption by greenhouse gases and clouds is more significant than the
28 LW scattering effect by clouds, most climate models neglect cloud LW scattering to save
29 computational costs. Ignoring cloud LW scattering directly overestimates outgoing longwave
30 radiation (OLR). This study included ice-cloud LW scattering treatment in the Exascale Energy
31 Earth System Model (E3SM) version 2 and ran fully-coupled simulations, prescribed sea surface
32 temperature simulations, and offline radiative transfer calculations to comprehensively assess the
33 impact of ice-cloud LW scattering on global climate simulation. The instantaneous effect due to
34 ice-cloud LW scattering reduces the OLR by $\sim 1 \text{ W/m}^2$ on the global average and 2 W/m^2 on the
35 tropical average. Tropospheric warming and high cloud amount reduction act to partially
36 compensate for such instantaneous OLR reduction caused by the inclusion of LW scattering. When
37 the simulation reaches the equilibrium, the surface warms by 0.66 K on average with respect to
38 the simulation without LW scattering, with the Arctic surface temperature differences more than
39 twice as large as that of the global mean. The impact of including LW scattering on the simulated
40 climate change in response to $4\times\text{CO}_2$ is also assessed. While including the cloud LW scattering
41 does not significantly modify radiative forcing and total radiative feedback under such a scenario,
42 it results in a 10% more positive cloud feedback.

43

44 **Plain Language Summary**

45 Clouds are an essential mediator in the climate system because they can reflect solar radiation back
46 to space and block longwave radiation emitted below reaching the top of the atmosphere by either
47 absorbing it or scattering it elsewhere. Such longwave scattering physics is deemed less important
48 and thus neglected in most climate models to save computational time. We incorporated this
49 mechanism into a climate model and ran pairs of simulations, with or without cloud scattering, to
50 see how it would affect the simulated global climate. We found that cloud longwave scattering
51 reduces the longwave radiation that goes to space. Such reduction of outgoing longwave radiation
52 is strongest in the tropics. Compared to the simulation without longwave scattering, the mean-state
53 surface temperature change is larger in the Arctic than in the tropics, which is primarily caused by
54 the slow response to the inclusion of scattering. We also assessed to what extent the inclusion of
55 cloud longwave scattering can affect the simulated response to abrupt $4\times\text{CO}_2$ increase. We
56 concluded that it can increase the cloud feedback strength by $\sim 10\%$, but overall, the impact is not
57 statistically significant.

58

59 **1. Introduction**

60 Clouds play an important role in the climate system (Stephens, 2005; and references therein).
61 Despite its importance in the climate system, cloud feedbacks still remain the largest uncertainty
62 in climate feedback estimation (Sherwood et al., 2020). This is partly due to the multi-scale
63 complexity of cloud processes, its intricate connections with large-scale dynamics, radiation, and
64 cloud microphysics, and the oversimplification or exclusion of known physical processes by the
65 climate models due to various computational constraints.

66 Cloud longwave (LW) scattering is one of such oversimplified or excluded physical processes in
67 climate models. The cloud scattering effect is believed to be secondary in the LW due to strong
68 absorption by greenhouse gases and clouds. As a result, the majority of climate models neglect
69 LW scattering to save computational costs (Chen et al., 2020; Kuo et al., 2020). Earlier studies
70 used offline radiative transfer calculation to show that omitting cloud LW scattering can lead to an
71 overestimation of outgoing longwave radiation (OLR) (Stephens, 1980). Photons scattered by
72 clouds will take a longer path to reach the top of the atmosphere (TOA), increasing the probability
73 of being absorbed by greenhouse gas molecules, cloud particles, or the surface. This can further
74 lead to a different atmospheric radiative cooling rate and a different surface downward LW flux
75 (FLDS) (Ritter & Geleyn, 1992). Several parameterization schemes have been proposed to include
76 multiple scattering of LW fluxes by clouds in climate models (Chou et al., 1999; Fu et al., 1997;
77 Li & Fu, 2000). Using atmospheric profiles from model simulations or reanalysis, these studies
78 estimated that when cirrus LW scattering is included, the instantaneous OLR can be reduced by

79 6~8 W/m² under the overcast conditions, and the FLDS can be increased by 2~4 W/m²
80 correspondingly. (Chou et al., 1999; Fu et al., 1997; Joseph & Min, 2003; Ritter & Geleyn, 1992).
81 Aside from cirrus clouds, which were believed to induce the most prominent LW scattering effect,
82 some studies also highlighted the importance of scattered LW fluxes for radiation budget over the
83 marine stratocumulus cloud regions (Costa & Shine, 2006; Kuo et al., 2017; Schmidt et al., 2006).
84 It was estimated that, without LW scattering, the global mean OLR is overestimated by 1.5~3
85 W/m² (Costa & Shine, 2006; Kuo et al., 2017).

86 Beyond estimating the direct impact of cloud LW scattering on the radiation budget, efforts have
87 been made to include cloud LW scattering in climate models to investigate how this can affect the
88 overall simulated climate (Jin et al., 2019; Zhao et al., 2018). By examining prescribed sea surface
89 temperature (SST) simulations, they estimated a global-mean OLR reduction by ~2.6 W/m² when
90 the effect of cloud LW scattering is considered, which is 0.8 W/m² larger than the estimated
91 instantaneous effect. Zhao et al. (2018) attributed it to the water vapor increase in response to the
92 warming atmosphere. However, such prescribed-SST simulations cannot evaluate the impact of
93 cloud LW scattering on surface climate as the surface-atmosphere coupling is constrained. To
94 address this, Chen et al. (2020) used the Community Earth System Model (CESM) 1.1 slab-ocean
95 model with a modified LW scheme to study the ice cloud LW scattering effect. They argued that
96 cloud LW scattering is especially important over polar regions due to the small amount of water
97 vapor in such regions. Their simulations showed a 1.0~2.0 K increase in the seasonal-mean surface
98 air temperature over the polar region, which is at least twice as much as the increase in the tropics.

99 Such temperature increases in the polar regions are mostly absent in their prescribed-SST
100 simulations, highlighting the importance of surface-atmosphere coupling when evaluating the
101 impact of cloud LW scattering on simulated climate. However, the analysis by Chen et al. (2020)
102 is largely confined to the polar region without examining possible connections between extra-polar
103 and polar regions (Holland & Bitz, 2003; Stuecker et al., 2018).

104 To the best of our knowledge, no study has run fully-coupled simulations to assess the effect of
105 cloud LW scattering on the simulated climate. Unlike the slab-ocean models that do not include
106 ocean dynamics and prescribe the meridional heat transport by oceans, the fully-coupled models
107 have full ocean dynamics. They thus can represent the ocean's responses better. With these
108 simulations, we can analyze the fast adjustment (i.e., atmospheric and land processes when SST is
109 fixed) and slow adjustment (i.e., when SST is allowed to change) in response to the initial TOA
110 flux change caused by cloud LW scattering. Previous modeling studies have also limited their
111 scope to the mean state climate difference after including cloud LW scattering. Modification of
112 cloud optics could affect how the climate system responds to the increase of greenhouse gases. In
113 this study, we incorporate the same ice-cloud LW scattering treatment in Chen et al. (2020) into
114 the Exascale Energy Earth System Model (E3SM) version 2, a flagship climate model developed
115 by the Department of Energy (Golaz et al., 2022). Note that LW scattering by liquid water clouds
116 is not included here to be consistent with the treatment in Chen et al. (2020). The OLR reduction
117 caused by liquid cloud LW scattering is only $\sim 1/2$ of the reduction caused by ice cloud LW
118 scattering, although the FLDS increase caused by them is comparable (Kuo et al., 2017). This

119 study focuses on understanding the impact of ice cloud LW scattering, which also includes the LW
120 scattering of the ice portion of mixed-phase clouds. Hereafter, cloud LW scattering refers to ice
121 cloud LW scattering only. Using the modified model, we ran fully coupled simulations and
122 prescribed-SST simulations with cloud LW scattering on and off to evaluate how the inclusion of
123 cloud LW scattering can affect the simulated mean-state climate. The central question to answer
124 is that, for a climate model without scattering, how the fast process (i.e., direct atmospheric
125 responses) and slow processes respond to the inclusion of LW scattering to attain a new mean state.
126 Moreover, we ran additional pairs of $4\times\text{CO}_2$ simulations, with LW scattering on and off, to
127 investigate how enabling cloud LW scattering affects the simulated radiative feedback and climate
128 sensitivity.

129 Section 2 describes the model we used, our modifications, and the details of the numerical
130 experiments. After a brief analysis of the total mean-climate state change when cloud LW
131 scattering is included in section 3, section 4 delineates the instantaneous effect due to the inclusion
132 of cloud LW scattering, the fast response to such instantaneous effect, and the relationship between
133 them. The impact on radiative feedback and long-term surface temperature change, as seen in the
134 suites of $4\times\text{CO}_2$ experiments, is investigated in section 5, followed by a conclusion and discussion
135 section.

136 **2. Model, Data and Methods**

137 **2.1. E3SM version 2**

138 E3SMv2 (Golaz et al., 2022) is the successor of the first version of the E3SM model (E3SMv1)
139 developed by the Department of Energy (Golaz et al., 2019). Although the first version was
140 initially branched from CESM1, the second one is different from CESM as many components have
141 been replaced or heavily modified, including the atmosphere dynamical core, ocean model, sea ice
142 model, and river routing. Atmospheric physics in E3SMv2 still shares similarities with CESM2.
143 To evaluate the model, the E3SM team conducted experiments according to a standard set of the
144 Coupled Model Intercomparison Project Phase 6 (CMIP6) Diagnosis, Evaluation, and
145 Characterization of Klima (DECK) simulations (Eyring et al., 2016). Compared to its predecessor,
146 E3SMv2 doubles its speed and alleviates some issues. For example, it simulates better clouds and
147 precipitation climatology and, consequently, improves the estimates of cloud feedbacks and
148 equilibrium climate sensitivity (ECS). While E3SMv1 estimates an ECS of 5.3 K, which is deemed
149 too high, E3SMv2 estimates a more realistic ECS value of 4.0 K (Golaz et al., 2022).

150 Our new fully-coupled simulations were branched from year 101 of the 500-year E3SMv2 pre-
151 industrial control run (v2.LR.piControl), one of the standard runs in the CMIP6 DECK experiment.
152 These simulations run on a horizontal grid of ~ 100 km in the atmosphere and land components, $\frac{1}{2}$
153 degree in the river component, and 60 to 30 km in the ocean and sea-ice components. The
154 atmosphere has 72 vertical layers from the surface to approximately 60 km. Note that the model
155 runs on separate dynamics and column parameterization grids to improve computational efficiency.
156 As a result, the dynamics grid has an average horizontal grid of 110 km, while the parameterization
157 grid and the land grid have an average grid size of 165 km.

158 **2.2. Model modifications to enable ice-cloud LW scattering**

159 This study employed the same ice-cloud optics and longwave radiation schemes as described in
160 Chen et al. (2020). In brief, a hybrid two-stream and four-stream (2S/4S) radiative transfer solver
161 is implemented into the LW radiation scheme to enable cloud LW scattering. Compared to other
162 solvers, the hybrid 2S/4S solver has a better compromise between accuracy and computational
163 efficiency (Fu et al., 1997). The default ice-cloud optics in the E3SMv2 do not include ice-cloud
164 scattering properties in the LW. In this study, cloud optical properties, including cloud extinction
165 coefficients, single-scattering albedo, and asymmetry factors, are based on a cloud habit model
166 (Yang et al., 2018) consistent with that used for the Moderate Resolution Imaging
167 Spectroradiometer (MODIS) Collection 6 operational cloud products (Platnick et al., 2015; 2017).
168 When cloud LW scattering is disabled, the extinction coefficient is set equal to the absorption
169 coefficient. Details about the LW radiative transfer solver and ice-cloud optics can be found in
170 Kuo et al. (2020) and Chen et al. (2020).

171 **2.3. Numerical experiment design and data analysis**

172 The scheme described in the previous subsection has been ported to the E3SMv2. We carried out
173 four fully-coupled simulations, each one consisting of 105 years (i.e., year 0101 ~ 0205):

- 174 • Control: fully-coupled simulation without cloud LW scattering;
- 175 • Scat: fully-coupled simulation with cloud LW scattering;
- 176 • Control_4xCO₂: same as Control, but the CO₂ concentration is set to four times of the
177 piControl value, i.e., instantaneous quadrupling CO₂ experiment.

- 178 • Scat_4xCO2: same as Scat, but the CO₂ concentration is set to four times of the piControl
179 value.

180 The other specifications of the four simulations are identical. By comparing the Scat case and the
181 Control case, we can study the effects of cloud LW scattering on the simulated mean climate. With
182 4xCO₂ cases, we can further contrast climate feedbacks when cloud LW scattering is enabled or
183 disabled. Note that the Control run is not the same as the standard E3SMv2 piControl run because
184 the default ice-cloud optics are replaced with MODIS Collection 6 ice optics, and the radiative
185 transfer solver is replaced by the hybrid 2S/4S solver with the LW scattering capability.

186 Figure 1 shows the time series of global-mean net TOA radiative flux imbalance and surface
187 temperature of the four simulations. Because we replaced the ice-cloud optics and the radiative
188 transfer solver, the Control run has a small TOA energy loss after branching from the equilibrated
189 piControl run. Long-term mean TOA energy imbalance is -0.19 W/m². The Scat case, on the other
190 hand, is closer to the equilibrium state (-0.01 W/m²). The difference in surface temperature
191 between the Scat and the Control case accumulates to ~0.6 K after about 30 years. Both
192 Control_4xCO₂ and Scat_4xCO₂ have more than 1 W/m² net TOA energy imbalance throughout
193 the simulations. However, the surface temperature in both cases becomes stable after about 70
194 years. For the last 30 years (year 0176 ~ 0205), the absolute trend of net TOA energy imbalance
195 in all simulations is less than 0.02 W/m² per year, and the absolute trend of surface temperature is
196 within 0.01 K per year. Therefore, we used the last 30 years of those simulations in all climatology

197 calculations in the following sections. Note that the difference in global-mean surface temperature
198 (Fig. 1b) between Scat and Control is similar to that between Scat_4xCO2 and Control_4xCO2.

199 **3. Impact on Mean State Climate**

200 **3.1. Total Response in Equilibrium**

201 Compared to a simulated climate system without LW scattering, the instantaneous effect of LW
202 scattering is to reduce the global-mean OLR (Costa & Shine, 2006; Kuo et al., 2017). Therefore,
203 more energy would be retained in the climate system and a warming climate can be expected.

204 Figure 2 summarizes the impacts on the surface climatology due to cloud LW scattering, where
205 the differences in global mean surface air temperature and downward longwave flux at surface
206 (FLDS) are plotted in each row. Panels (b) and (d) show the zonal mean differences of the
207 corresponding variables. In addition to the annual mean value (black), these panels also show the
208 changes in boreal summers (red) and boreal winters (blue). Globally speaking, the cloud LW
209 scattering effect results in a warmer surface by 0.66 K on average. The largest warming occurs in
210 the Arctic, where the annual-mean maximum exceeds 2 K. It is amplified in winters (~4 K) and
211 damped in summers (~0.5 K). Such seasonal variation is a typical feature of the polar amplification
212 phenomenon and can be explained by feedback processes in the Arctic region (Stuecker et al.,
213 2018; Boeke et al., 2021). Correspondingly, FLDS increases by approximately 4 W/m² on global
214 average. Its high correlation with surface air temperature is also consistent with what Chen et al.
215 (2020) has revealed.

216 Figure 3(a-c) shows the vertical temperature profile difference when the cloud LW scattering effect
217 is enabled. For pure comparison purpose, the differences caused by the 4×CO₂ effect are also
218 presented in Figure 3(d-f). Please note Figure 3(a-c) is the mean-state difference caused by
219 including a physical process in the model while Figure 3(d-f) is the difference caused by abrupt
220 4×CO₂ increases in the original model without LW scattering. Regardless of the scale difference
221 (2 K versus 20 K), they share some common features including the large warming of the upper
222 troposphere in the tropics (Manabe & Wetherald, 1975; Manabe & Stouffer, 1980) and the confined
223 near-surface warming in the Arctic. However, when cloud LW scattering is activated, the
224 stratosphere does not cool as much as the one in the case of 4×CO₂ concentration. This can be
225 explained by the fact that CO₂ has a strong stratospheric radiative cooling effect and, thus, increase
226 of CO₂ directly affect the radiative equilibrium in the stratosphere; but enabling cloud longwave
227 scattering would not directly affect the radiative cooling in the stratosphere.

228 **3.2. Instantaneous Radiative Effect and Fast Response**

229 Analogous to the concepts in radiative forcing and feedback analysis, in this section, we
230 decomposed the total TOA flux changes (i.e., *total response*) due to the inclusion of cloud LW
231 scattering into three parts: *instantaneous radiative effect* (analogous to IRF, instantaneous radiative
232 forcing), *fast adjustment* (corresponding to rapid adjustment), and *slow adjustment*. The sum of
233 the first two parts is termed the *fast response* (analogous to ERF, effective radiative forcing). We
234 also decomposed FLDS into the same three parts to attribute the FLDS increase to physical
235 processes.

236 The instantaneous radiative effect is defined as the radiative flux change when we only include the
237 cloud LW scattering physics; all atmospheric and surface state variables are fixed. In this case,
238 shortwave flux is unmodified. Similar to the approach in Zhao et al. (2018) to quantitatively derive
239 the scattered LW flux by clouds, we ran a short 3-year simulation configured similar to the Scat
240 case. While these runs evolve with cloud LW scattering enabled, the model outputs additional
241 longwave radiative fluxes and longwave heating rates computed in parallel but without the cloud
242 LW scattering effect. The instantaneous radiative effect is the difference between these extra
243 outputs (without scattering) and the original flux outputs (with scattering). Over the course of three
244 years, this difference shows a small seasonal variation ($\sim 1 \text{ W/m}^2$ for OLR and $\sim 0.2 \text{ W/m}^2$ for FLDS)
245 and an even smaller annual variation (Figure S1). Hence, we think this derived instantaneous
246 radiative effect is applicable to interpret our fully-coupled simulation results.

247 Figure 4 shows the zonal mean instantaneous OLR change and FLDS change, as well as the total
248 response, due to the cloud LW scattering effect. Here, cloud LW scattering reduces the OLR by
249 1.13 W/m^2 globally on average. The largest decrease is seen in the tropics by 2 W/m^2 , while the
250 smallest decrease occurs in the polar region and the subtropical region ($< 1 \text{ W/m}^2$). Such latitudinal
251 distribution is consistent with Kuo et al. (2017) and Costa & Shine (2006). Note that the
252 instantaneous FLDS increase due to the scattered LW flux by ice clouds is only 0.08 Wm^{-2} , only
253 $\sim 2\%$ of the FLDS increase for the total response (3.95 W/m^2 globally), suggesting that climate
254 feedbacks must play an important role in the change of FLDS.

255 Fast response here is defined as the TOA flux changes when SST and sea ice conditions are fixed.
256 This is equal to the instantaneous radiative effect plus the fast adjustment due to changes in
257 atmospheric temperature, land temperature, water vapor concentration, and clouds. To derive this
258 quantity, we ran two 35-year prescribed-SST simulations, one with cloud LW scattering and one
259 without. Only the atmosphere component is active, while SST and sea ice are prescribed using
260 historical observations from 1980 to 2014. The zonal mean OLR and FLDS differences between
261 these two runs are plotted as blue curves in Figure 4. We also calculated the contributions to the
262 flux changes from individual components of the atmosphere-surface system using a radiative
263 kernel (Huang et al., 2017) except clouds. Cloud adjustments are directly calculated from all-sky
264 and clear-sky fluxes output from the model. The impact on the TOA fluxes is summarized in Table
265 1.

266 Following the instantaneous OLR reduction due to the LW scattering effect, fast adjustments
267 increase the OLR by 0.44 W/m^2 . The sum of individual fast adjustment terms is 0.45 W/m^2 , close
268 to the amount above, which confirms the validity of using a radiative kernel to decompose the fast
269 adjustment. Major contributors to the OLR increase include cloud LW radiative effect (0.283
270 W/m^2), tropospheric warming (0.260 W/m^2), and land surface warming (0.028 W/m^2).
271 Stratospheric temperature change only leads to a small change in OLR by -0.013 W/m^2 . This
272 phenomenon is a typical feature of increased absorption in the troposphere but nearly unchanged
273 absorption in the stratosphere, as this is comparable to the pattern of the rapid adjustment when
274 black carbon is injected into the troposphere (Smith et al., 2018). Consequently, the TOA flux

275 imbalance becomes smaller, and the peak in the tropics is also shaved (Figure 4a). The FLDS
276 change after fast adjustments increases by 0.35 W/m^2 , primarily due to tropospheric warming
277 (Figure 4b). The increase in the Arctic is larger than the global mean ($\sim 1 \text{ W/m}^2$).

278 As for the slow adjustment to further compensate for the TOA flux imbalance of 0.67 W/m^2 (the
279 imbalance caused by the instantaneous effect of the inclusion of cloud LW scattering and the fast
280 response to such inclusion together), it consists of the surface temperature increase and the
281 subsequent state variable changes via various feedback mechanisms. As a result, the global-mean
282 OLR in the Scat case now exceeds the one in the Control case (Figure 4a) and the global-mean
283 shortwave flux in the Scat case is smaller than it in the control case (thus the net TOA imbalance
284 becomes closer to zero). Ultimately, cloud LW scattering induces a small warming effect globally.

285 The ratio of net TOA flux changes and surface temperature increase (0.66 K) in the slow process
286 is approximately $-0.9 \text{ W/m}^2/\text{K}$, a value that is close to the one in the case of CO_2 concentration
287 increase (which will be discussed in the next section). Driven by surface warming, FLDS in total
288 response is significantly stronger, especially in the Arctic where the magnitude exceeds 10 W/m^2
289 (Figure 4b). This suggests that the large increase of FLDS in the Arctic is dominantly caused by
290 the slow adjustment. Because of the positive correlation between FLDS and TS, it can be inferred
291 that the strong warming in the Arctic region should be attributed to the slow adjustments instead
292 of the instantaneous radiative effect. Total responses seen in cloud fraction and properties are also
293 the consequence of slow adjustments, including ice-to-liquid transition in tropical mid-troposphere
294 (Figure S2), elevated deep convective clouds (Figure S3), reduced anvil cloud coverage (Figure

295 S3), and increased stratiform low cloud coverage (Figure S4).

296 **4. Impact on the Simulated Climate Change Under 4×CO₂ Scenario**

297 In addition to the impact on the simulated mean-state climatology, a more scientifically intriguing
298 question is to what extent the inclusion of cloud LW scattering can affect the simulated climate
299 change in response to the increase of greenhouse gases. This section discusses this effect in the
300 context of abrupt 4×CO₂ simulations.

301 We adopted the regression approach to calculate the ERF and total climate feedback for the cases
302 with or without cloud LW scattering (Gregory et al., 2004). Figure 5 shows the scatterplot of
303 annual-mean net TOA radiation with respect to surface temperature (a.k.a., Gregory plot) for both
304 cases. The scatter points for both Control and Scat cases mix with each other. While the inclusion
305 of cloud LW scattering tends to decrease the ERF and increase the total feedback, the differences
306 are statistically negligible: the slopes of two corresponding regression lines (i.e., Control and Scat)
307 only differ by 0.03 W/m²/K, with a large overlap between their 95% confidence intervals (i.e., -
308 0.74±0.08 vs -0.71±0.09 W/m²/K); the intercept difference is 0.24 W/m², also with a large overlap
309 between their 95% confidence intervals (i.e., 6.28±0.49 vs 6.04±0.54) W/m². Thus, two regression
310 results are statistically indistinguishable. Consistent with such assessment, the global-mean surface
311 temperature changes due to 4×CO₂, as inferred from the last 30 years of simulations (Figure 1),
312 are 6.8 K for the Control case and 6.7 K for the Scat case, also suggesting that the cloud LW
313 scattering affects little on such climate projection simulation.

314 To gain a detailed understanding of how the LW scattering affects individual radiative feedback
315 strength, we decompose the total feedback into different components using the radiative kernel
316 approach. We employed the same radiative kernel used in Section 4 to derive Planck feedback,
317 lapse rate feedback, water vapor feedback, and surface albedo feedback. Cloud feedbacks are
318 calculated using cloud radiative kernels similar to Zelinka et al. (2012a; 2012b). As the kernel in
319 Zelinka et al. (2012a, 2012b) was built without LW cloud scattering, we calculated a correction
320 term based on offline radiative transfer calculations with LW scattering turning on and off, and
321 derive two sets of LW cloud radiative kernels using the approach described in Zelinka et al. (2012a).
322 Then, we took the difference between the two kernels and deemed it as the correction term to the
323 original Zelinka’s LW cloud radiative kernel. Figure 6a visualizes the kernel without cloud LW
324 scattering, and figure 6b shows the correction term. The correction term can exceed 10% for high
325 cloud with optical depth ≤ 3.6 .

326 Figure 7 summarizes the decomposition of the total radiative feedback into individual terms. Two
327 sets of cloud feedback are included using the original cloud radiative kernel and the new kernel
328 with the correction term. Accounting for the correction due to cloud LW scattering, the largest
329 absolute change in individual terms is the cloud feedback. Both LW and SW parts contribute to the
330 increase in cloud feedback, together adding $\sim 10\%$ of the total cloud feedback strength to the
331 counterpart derived from the Control simulations (i.e., without cloud LW scattering). Lapse rate
332 feedback and water vapor feedback are also modified when cloud LW scattering is included, but
333 these changes almost cancel out. Surface albedo feedback also decreases by approximately 0.03

334 W/m²/K, or 6% of that in the Control case. With the correction term, the sum of changes from each
335 individual term has a much better agreement with the change in total feedback strength estimated
336 from the regression method (lower right panel in Fig. 7). Nevertheless, given the uncertainty of
337 climate feedback estimation and because the ice cloud LW scattering effect on feedback terms is
338 small in magnitude, few differences shown in Fig. 7 are likely to be statistically significant.

339 **5. Conclusions**

340 We modified the E3SM version 2, a fully-coupled climate model, to include the ice cloud LW
341 scattering effect, a physical process omitted by most climate models. Based on the modified model,
342 we ran simulations with our modifications enabled and disabled to study the impact of ice cloud
343 LW scattering on the simulated climate system, for both the mean-state and climate-change
344 simulations. Figure 8 summarizes the radiative and temperature responses to the inclusion of ice
345 cloud LW scattering.

346 Compared to the simulation without longwave scattering, the instantaneous radiative effect due to
347 ice cloud LW scattering reduces the OLR (outgoing longwave radiation) across all latitudes. The
348 strongest OLR reduction occurs in the tropics. Most scattered fluxes are absorbed in the
349 atmosphere instead of reflected to the surface, as the instantaneous increase of FLDS (downward
350 longwave radiative flux at the surface) is negligible compared to the OLR reduction. The OLR
351 reduction is compensated to some extent, primarily by the warming troposphere and cloud LW
352 effect through fast adjustments. Stratosphere contributes little here as the LW scattering alters the
353 radiative flux throughout the troposphere but has little effect on the stratosphere. The majority of

354 the total FLDS increase, as well as the highly correlated surface temperature increase, is primarily
355 due to the slow adjustment. Consequently, compared to the mean-state climate simulated by the
356 model without LW scattering, the global-mean surface temperature difference is +0.66 K, with the
357 difference in the Arctic at least twice as much as the global mean difference, especially in boreal
358 winter.

359 In the scenario of abrupt $4\times\text{CO}_2$ simulations, ice cloud LW scattering does not significantly modify
360 ERF (effective radiative forcing) and climate feedbacks. The ERF and total feedback strengths
361 inferred from two pairs of simulations, with and without ice cloud LW scattering, has no
362 statistically significant differences. When total feedback is decomposed to individual feedback
363 using the radiative kernel technique, the most notable change is the 10% increase of cloud feedback
364 due to the inclusion of ice cloud LW scattering. Such a change might not be statistically significant,
365 though, given the uncertainty of cloud feedback.

366 This study refines and deepens our understanding of the cloud LW scattering effect. The
367 explanation in Chen et al. (2020) for the simulated responses of mean states in the polar region
368 overlooked the global connections, especially the changes in the tropics caused by cloud LW
369 scattering. We took advantage of fully-coupled simulations, prescribed simulations, and offline
370 radiative transfer calculations to analyze the instantaneous effect, fast adjustment, and slow
371 adjustment after including the scattering physics. These analyses delineate a full picture of how
372 the inclusion of cloud LW scattering affects the simulation of the mean-state climate. This study
373 revealed that the strong response in the Arctic is primarily due to the highly sensitive nature of the

374 polar climate. The instantaneous OLR reduction due to cloud LW scattering is indeed relatively
375 weak in the Arctic. In addition, we assessed how including cloud LW scattering physics can affect
376 ERF and climate feedbacks caused by the increase of CO₂. While the impacts on the ERF and
377 climate feedbacks are statistically insignificant, the cloud LW scattering is more inclined to
378 increase the total feedback via more positive cloud feedback. Note that liquid cloud LW scattering
379 is not studied here. Considering the different spatial distributions of ice clouds and liquid clouds,
380 liquid cloud LW scattering effect may have different structural impacts on mean-state climate and
381 climate feedback. Future work is warranted to assess the impact of liquid cloud LW scattering on
382 climate simulations.

383 Cloud LW scattering is one example of physical processes that are often neglected in climate
384 modeling studies. A variety of compensating biases occur in any fully-coupled climate model
385 simulations. The inclusion of cloud LW scattering reduce one type of structural uncertainties in the
386 climate models. While such reduction of structural uncertainties might not directly lead to an
387 improved climate simulations (as the modified model might needs to be re-tuned), it could help
388 expose other compensating errors. Future work is warranted to compare the historical runs based
389 on this modified model to satellite observations and reanalysis products. It can also be beneficial
390 in future studies to include cloud LW scattering in other climate models and assess the impact on
391 multi-model mean state as well as individual model simulation. In terms of computational costs,
392 the modifications cost 10% additional computational time compared to the original E3SMv2
393 model.

394 Because of the three-dimensional nature of scattering, it would be a meaningful follow-up study
395 to examine the cloud LW scattering effect in the context of 3D radiative transfer (e.g., Kablick et
396 al., 2011), especially for high-spatial-resolution global simulations such as those global storm-
397 resolving models with a spatial resolution as high as 1~3 km (Stevens et al., 2019). The horizontal
398 photon flux transport, which is entirely neglected in plane-parallel radiative transfer calculation,
399 could become important for certain cloud regimes (e.g., cumulus and stratocumulus) in such global
400 storm-resolving model simulations.

401 **Acknowledgment**

402 We thank the Editor, the Associate Editor, and three reviewers for their constructive and insightful
403 comments, which greatly increase the clarity and intellectual value of this study. This material is
404 based upon work supported by the U.S. Department of Energy, Office of Science, Office of
405 Biological and Environmental Research, Climate and Environmental Science Division under
406 Awards DE-SC0019278 and DE-SC0022117 to the University of Michigan with a subcontract to
407 Texas A&M. YHC performed relevant work for this project entirely during his stay at the
408 University of Michigan. We wish to thank Dr. Xianwen Jing for his contribution to code
409 development during his postdoctoral stay at the University of Michigan. CXF also acknowledges
410 the support from the NASA FINNEST program under Grant No. 80NSSC22K1433 for part of the
411 studies presented here.

412 **Open Research**

413 The source code of the original E3SM version 2 can be found in a publicly accessible repository
414 (E3SM Project, 2021; Golaz et al., 2022). The source code of our modified model is currently
415 preserved on Zenodo (Fan et al., 2023). The Control run can be reproduced using the
416 cxfan/v2.LR.piControl.0101.UMRad.CTRL branch, and the Scat run using the
417 cxfan/v2.LR.piControl.0101.UMRad.Scat branch. Model outputs were processed using netCDF
418 Operator (NCO; Zender, 2022) and xarray v2023.02.0 (Hoyer & Hamman, 2017; Hoyer et al.,
419 2023). The radiative kernel used to decompose individual feedback terms can be downloaded from
420 Mendeley Data archive (Huang, 2022; Huang et al., 2017). Figures were produced with Matplotlib
421 version 3.6.3 (Caswell et al., 2020; Hunter, 2007).

422 **References**

- 423 Boeke, R. C., Taylor, P. C., & Sejas, S. A. (2021). On the Nature of the Arctic's Positive Lapse-
424 Rate Feedback. *Geophysical Research Letters*, 48(1). <https://doi.org/10.1029/2020gl091109>
- 425 Bony, S., Stevens, B., Coppin, D., Becker, T., Reed, K. A., Voigt, A., & Medeiros, B. (2016).
426 Thermodynamic control of anvil cloud amount. *Proceedings of the National Academy of*
427 *Sciences*, 113(32), 8927–8932. <https://doi.org/10.1073/pnas.1601472113>
- 428 Caswell, T. A., Lee, A., Droettboom, M., Andrade, E. S., Hoffmann, T., Klymak, J., et al.
429 (2020). matplotlib/matplotlib: REL: v3.6.3 [Software]. Zenodo.
430 <https://doi.org/10.5281/zenodo.7527665>

431 Chen, Y., Huang, X., Yang, P., Kuo, C., & Chen, X. (2020). Seasonal Dependent Impact of Ice
432 Cloud Longwave Scattering on the Polar Climate. *Geophysical Research Letters*, 47(23).
433 <https://doi.org/10.1029/2020gl090534>

434 Chou, M.-D., Lee, K.-T., Tsay, S.-C., & Fu, Q. (1999). Parameterization for Cloud Longwave
435 Scattering for Use in Atmospheric Models. *Journal of Climate*, 12(1), 159–169.
436 [https://doi.org/10.1175/1520-0442\(1999\)012<0159:pfclsf>2.0.co;2](https://doi.org/10.1175/1520-0442(1999)012<0159:pfclsf>2.0.co;2)

437 Costa, S. M. S., & Shine, K. P. (2006). An estimate of the global impact of multiple scattering by
438 clouds on outgoing long-wave radiation. *Quarterly Journal of the Royal Meteorological*
439 *Society*, 132(616), 885–895. <https://doi.org/10.1256/qj.05.169>

440 E3SM Project, DOE. (2021). Energy Exascale Earth System Model v2.0. [Software].
441 <https://doi.org/10.11578/E3SM/dc.20210927.1>.

442 Eyring, V., Bony, S., Meehl, G. A., Senior, C. A., Stevens, B., Stouffer, R. J., & Taylor, K. E.
443 (2016). Overview of the Coupled Model Intercomparison Project Phase 6 (CMIP6)
444 experimental design and organization. *Geoscientific Model Development*, 9(5), 1937–1958.
445 <https://doi.org/10.5194/gmd-9-1937-2016>

446 Fan, C., Chen, Y.-H., Chen, X., Lin, W., Yang, P., Huang, X., et al. (2023). cxfan1997/E3SM:
447 UMRad E3SMv2 First Release [Software]. Zenodo. <https://doi.org/10.5281/zenodo.7916862>

448 Fu, Q., Liou, K. N., Cribb, M. C., Charlock, T. P., & Grossman, A. (1997). Multiple Scattering
449 Parameterization in Thermal Infrared Radiative Transfer. *Journal of the Atmospheric*
450 *Sciences*, 54(24), 2799–2812. [https://doi.org/10.1175/1520-](https://doi.org/10.1175/1520-0469(1997)054<2799:mSPiTi>2.0.CO;2)
451 [0469\(1997\)054<2799:mSPiTi>2.0.CO;2](https://doi.org/10.1175/1520-0469(1997)054<2799:mSPiTi>2.0.CO;2)

452 Golaz, J.-C., Caldwell, P. M., Van Roekel, L. P., Petersen, M. R., Tang, Q., Wolfe, J. D., et al.
453 (2019). The DOE E3SM coupled model version 1: Overview and evaluation at standard
454 resolution. *Journal of Advances in Modeling Earth Systems*, 11, 2089–2129.
455 <https://doi.org/10.1029/2018MS001603>

456 Golaz, J.-C., Van Roekel, L. P., Zheng, X., Roberts, A. F., Wolfe, J. D., Lin, W., et al. (2022).
457 The DOE E3SM Model Version 2: Overview of the physical model and initial model
458 evaluation. *Journal of Advances in Modeling Earth Systems*, 14, e2022MS003156.
459 <https://doi.org/10.1029/2022MS003156>

460 Gregory, J. M., Ingram, W. J., Palmer, M. A., Jones, G. S., Stott, P. A., Thorpe, R. B., et al.
461 (2004). A new method for diagnosing radiative forcing and climate sensitivity. *Geophysical*
462 *Research Letters*, 31(3), L03205. <https://doi.org/10.1029/2003gl018747>

463 Hartmann, D. L., & Short, D. A. (1980). On the Use of Earth Radiation Budget Statistics for
464 Studies of Clouds and Climate. *Journal of the Atmospheric Sciences*, 37(6), 1233–1250.
465 [https://doi.org/10.1175/1520-0469\(1980\)037<1233:otuoer>2.0.CO;2](https://doi.org/10.1175/1520-0469(1980)037<1233:otuoer>2.0.CO;2)

466 Hartmann, D. L. & Larson, K. (2002). An important constraint on tropical cloud - climate
467 feedback. *Geophysical Research Letters*, 29, 1951. <https://doi.org/10.1029/2002GL015835>

468 Holland, M. M., & Bitz, C. M. (2003). Polar amplification of climate change in coupled models.
469 *Climate Dynamics*, 21, 221–232. <https://doi.org/10.1007/s00382-003-0332-6>

470 Hoyer, S. & Hamman, J., (2017). xarray: N-D labeled Arrays and Datasets in Python. *Journal of*
471 *Open Research Software*, 5(1), 10. <https://doi.org/10.5334/jors.148>

472 Hoyer, S., Roos, M., Joseph, H., Magin, J., Cherian, D., Fitzgerald, C., et al. (2023). xarray
473 (Version v2023.02.0) [Software]. Zenodo. <https://doi.org/10.5281/zenodo.7616056>

474 Huang, Y., Xia, Y., & Tan, X. (2017). On the pattern of CO₂ radiative forcing and poleward
475 energy transport. *Journal of Geophysical Research: Atmospheres*, 122(20), 10,578-10,593.
476 <https://doi.org/10.1002/2017jd027221>

477 Huang, Y. (2022). ERA-interim reanalysis based radiative kernels [Dataset], Mendeley Data.
478 <https://doi.org/10.17632/3drx8fmmz9.1>

479 Hunter, J. D. (2007). Matplotlib: A 2D Graphics Environment. *Computing in Science &*
480 *Engineering*, 9(3), 90-95. <https://doi.org/10.1109/MCSE.2007.55>.

481 Jin, Z., Zhang, Y., Genio, A. D., Schmidt, G., & Kelley, M. (2019). Cloud scattering impact on
482 thermal radiative transfer and global longwave radiation. *Journal of Quantitative*

483 *Spectroscopy and Radiative Transfer*, 239, 106669.
484 <https://doi.org/10.1016/j.jqsrt.2019.106669>

485 Joseph, E., & Min, Q. (2003). Assessment of multiple scattering and horizontal inhomogeneity in
486 IR radiative transfer calculations of observed thin cirrus clouds. *Journal of Geophysical*
487 *Research: Atmospheres*, 108, 4380. <https://doi.org/10.1029/2002jd002831>

488 Kablick, G. P., Ellingson, R. G., Takara, E. E., & Gu, J. (2011). Longwave 3D Benchmarks for
489 Inhomogeneous Clouds and Comparisons with Approximate Methods. *Journal of Climate* 24,
490 2192–2205. <https://doi.org/10.1175/2010jcli3752.1>

491 Klein, S.A., Hall, A., Norris, J.R., & Pincus, R. (2017). Low-Cloud Feedbacks from Cloud-
492 Controlling Factors: A Review. *Surveys in Geophysics*, 38, 1307–1329.
493 <https://doi.org/10.1007/s10712-017-9433-3>

494 Kuo, C., Yang, P., Huang, X., Feldman, D., Flanner, M., Kuo, C., & Mlawer, E. J. (2017).
495 Impact of Multiple Scattering on Longwave Radiative Transfer Involving Clouds. *Journal of*
496 *Advances in Modeling Earth Systems*, 9(8), 3082–3098.
497 <https://doi.org/10.1002/2017ms001117>

498 Kuo, C., Yang, P., Huang, X., Chen, Y., & Liu, G. (2020). Assessing the accuracy and
499 efficiency of longwave radiative transfer models involving scattering effect with cloud optical

500 property parameterizations. *Journal of Quantitative Spectroscopy and Radiative Transfer*,
501 240, 106683. <https://doi.org/10.1016/j.jqsrt.2019.106683>

502 Li, J., & Fu, Q. (2000). Absorption Approximation with Scattering Effect for Infrared Radiation.
503 *Journal of the Atmospheric Sciences*, 57(17), 2905–2914. [https://doi.org/10.1175/1520-0469\(2000\)057<2905:aawsef>2.0.co;2](https://doi.org/10.1175/1520-0469(2000)057<2905:aawsef>2.0.co;2)

504

505 Manabe, S., & Wetherald, R. T. (1975). The Effects of Doubling the CO₂ Concentration on the
506 climate of a General Circulation Model. *Journal of the Atmospheric Sciences*, 32(1), 3–15.
507 [https://doi.org/10.1175/1520-0469\(1975\)032<0003:teodtc>2.0.co;2](https://doi.org/10.1175/1520-0469(1975)032<0003:teodtc>2.0.co;2)

508 Manabe, S., & Stouffer, R. J. (1980). Sensitivity of a global climate model to an increase of CO₂
509 concentration in the atmosphere. *Journal of Geophysical Research: Oceans*, 85(C10), 5529–
510 5554. <https://doi.org/10.1029/jc085ic10p05529>

511 Mauritsen, T., & Stevens, B. (2015). Missing iris effect as a possible cause of muted
512 hydrological change and high climate sensitivity in models. *Nature Geoscience*, 8(5), 346–
513 351. <https://doi.org/10.1038/ngeo2414>

514 McCoy, D. T., Eastman, R., Hartmann, D. L., & Wood, R. (2017). The Change in Low Cloud
515 Cover in a Warmed Climate Inferred from AIRS, MODIS, and ERA-Interim. *Journal of*
516 *Climate*, 30(10), 3609–3620. <https://doi.org/10.1175/jcli-d-15-0734.1>

517 Platnick, S., Meyer, K. G., King, M. D., Wind, G., Amarasinghe, N., Marchant, B., et al. (2015).
518 *MODIS cloud optical properties: User guide for the collection 6 level-2 MOD06/MYD06*
519 *product and associated level-3 datasets, version 1.0*. Retrieved from [http://modis-atmos.gsfc.](http://modis-atmos.gsfc.nasa.gov/_docs/C6MOD06OPUserGuide.pdf)
520 [nasa.gov/_docs/C6MOD06OPUserGuide.pdf](http://modis-atmos.gsfc.nasa.gov/_docs/C6MOD06OPUserGuide.pdf)

521 Platnick, S., Meyer, K. G., King, M. D., Wind, G., Amarasinghe, N., Marchant, B., et al. (2017).
522 The MODIS Cloud Optical and Microphysical Products: Collection 6 Updates and Examples
523 from Terra and Aqua. *IEEE Transactions on Geoscience and Remote Sensing*, 55(1), 502–
524 525. <https://doi.org/10.1109/tgrs.2016.2610522>

525 Qu, X., Hall, A., Klein, S. A., & Caldwell, P. M. (2014). On the spread of changes in marine low
526 cloud cover in climate model simulations of the 21st century. *Climate Dynamics*, 42, 2603–
527 2626. <https://doi.org/10.1007/s00382-013-1945-z>

528 Ritter, B., & Geleyn, J.-F. (1992). A Comprehensive Radiation Scheme for Numerical Weather
529 Prediction Models with Potential Applications in Climate Simulations. *Monthly Weather*
530 *Review*, 120(2), 303–325. [https://doi.org/10.1175/1520-0493\(1992\)120<0303:acrsfn>2.0.co;2](https://doi.org/10.1175/1520-0493(1992)120<0303:acrsfn>2.0.co;2)

531 Schmidt, G. A., Ruedy, R., Hansen, J. E., Aleinov, I., Bell, N., Bauer, M., et al. (2006). Present-
532 Day Atmospheric Simulations Using GISS ModelE: Comparison to In Situ, Satellite, and
533 Reanalysis Data. *Journal of Climate*, 19(2), 153–192. <https://doi.org/10.1175/jcli3612.1>

534 Sherwood, S. C., Webb, M. J., Annan, J. D., Armour, K. C., Forster, P. M., Hargreaves, J. C., et
535 al. (2020). An Assessment of Earth's Climate Sensitivity Using Multiple Lines of Evidence.
536 *Reviews of Geophysics*, 58(4), e2019RG000678. <https://doi.org/10.1029/2019rg000678>

537 Smith, C. J., Kramer, R. J., Myhre, G., Forster, P. M., Soden, B. J., Andrews, T., et al. (2018).
538 Understanding Rapid Adjustments to Diverse Forcing Agents. *Geophysical Research Letters*,
539 45(21), 12023–12031. <https://doi.org/10.1029/2018gl079826>

540 Stephens, G. L. (1980). Radiative Properties of Cirrus Clouds in the Infrared Region. *Journal of*
541 *the Atmospheric Sciences*, 37(2), 435–446. [https://doi.org/10.1175/1520-](https://doi.org/10.1175/1520-0469(1980)037<0435:rpoeci>2.0.co;2)
542 0469(1980)037<0435:rpoeci>2.0.co;2

543 Stephens, G. L. (2005). Cloud Feedbacks in the Climate System: A Critical Review. *Journal of*
544 *Climate*, 18(2), 237–273. <https://doi.org/10.1175/jcli-3243.1>

545 Stevens, B., Satoh, M., Auger, L., Biercamp, J., Bretherton, C. S., Chen, X., et al. (2019).
546 DYAMOND: the DYNAMICS of the Atmospheric general circulation Modeled On Non-
547 hydrostatic Domains. *Progress in Earth and Planetary Science*, 6, 61.
548 <https://doi.org/10.1186/s40645-019-0304-z>

549 Stuecker, M. F., Bitz, C. M., Armour, K. C., Proistosescu, C., Kang, S. M., Xie, S.-P., et al.
550 (2018). Polar amplification dominated by local forcing and feedbacks. *Nature Climate*
551 *Change*, 8(12), 1076–1081. <https://doi.org/10.1038/s41558-018-0339-y>

552 Wood, R., & Bretherton, C. S. (2006). On the Relationship between Stratiform Low Cloud Cover
553 and Lower-Tropospheric Stability. *Journal of Climate*, 19(24), 6425–6432.
554 <https://doi.org/10.1175/jcli3988.1>

555 Yang, P., S. Hioki, M. Saito, C.-P. Kuo, B. A. Baum, K.-N. Liou, 2018: A review of ice cloud
556 optical property models for satellite remote sensing, *Atmosphere*, 9, 499.
557 <https://doi.org/10.3390/atmos9120499>

558 Yoshimori, M., Lambert, F. H., Webb, M. J. & Andrews, T. (2020). Fixed anvil temperature
559 feedback - positive, zero or negative? *Journal of Climate*, 33, 2719–2739.
560 <https://doi.org/10.1175/JCLI-D-19-0108.1>

561 Zelinka, M. D., & Hartmann, D. L. (2010). Why is longwave cloud feedback positive? *Journal*
562 *of Geophysical Research: Atmospheres*, 115, D16117. <https://doi.org/10.1029/2010jd013817>

563 Zelinka, M. D., & Hartmann, D. L. (2011). The observed sensitivity of high clouds to mean
564 surface temperature anomalies in the tropics. *Journal of Geophysical Research: Atmospheres*,
565 116, D23103. <https://doi.org/10.1029/2011jd016459>

566 Zelinka, M. D., Klein, S. A., & Hartmann, D. L. (2012a). Computing and Partitioning Cloud
567 Feedbacks Using Cloud Property Histograms. Part I: Cloud Radiative Kernels. *Journal of*
568 *Climate*, 25(11), 3715–3735. <https://doi.org/10.1175/jcli-d-11-00248.1>

- 569 Zelinka, M. D., Klein, S. A., & Hartmann, D. L. (2012b). Computing and Partitioning Cloud
570 Feedbacks Using Cloud Property Histograms. Part II: Attribution to Changes in Cloud
571 Amount, Altitude, and Optical Depth. *Journal of Climate*, 25(11), 3736–3754.
572 <https://doi.org/10.1175/jcli-d-11-00249.1>
- 573 Zender, C. S. (2022), netCDF Operator (NCO), Version 5.0.7 [Software].
574 <https://nco.sourceforge.net/>
- 575 Zhao, W., Peng, Y., Wang, B., & Li, J. (2018). Cloud Longwave Scattering Effect and Its Impact
576 on Climate Simulation. *Atmosphere*, 9(4), 153. <https://doi.org/10.3390/atmos9040153>
- 577

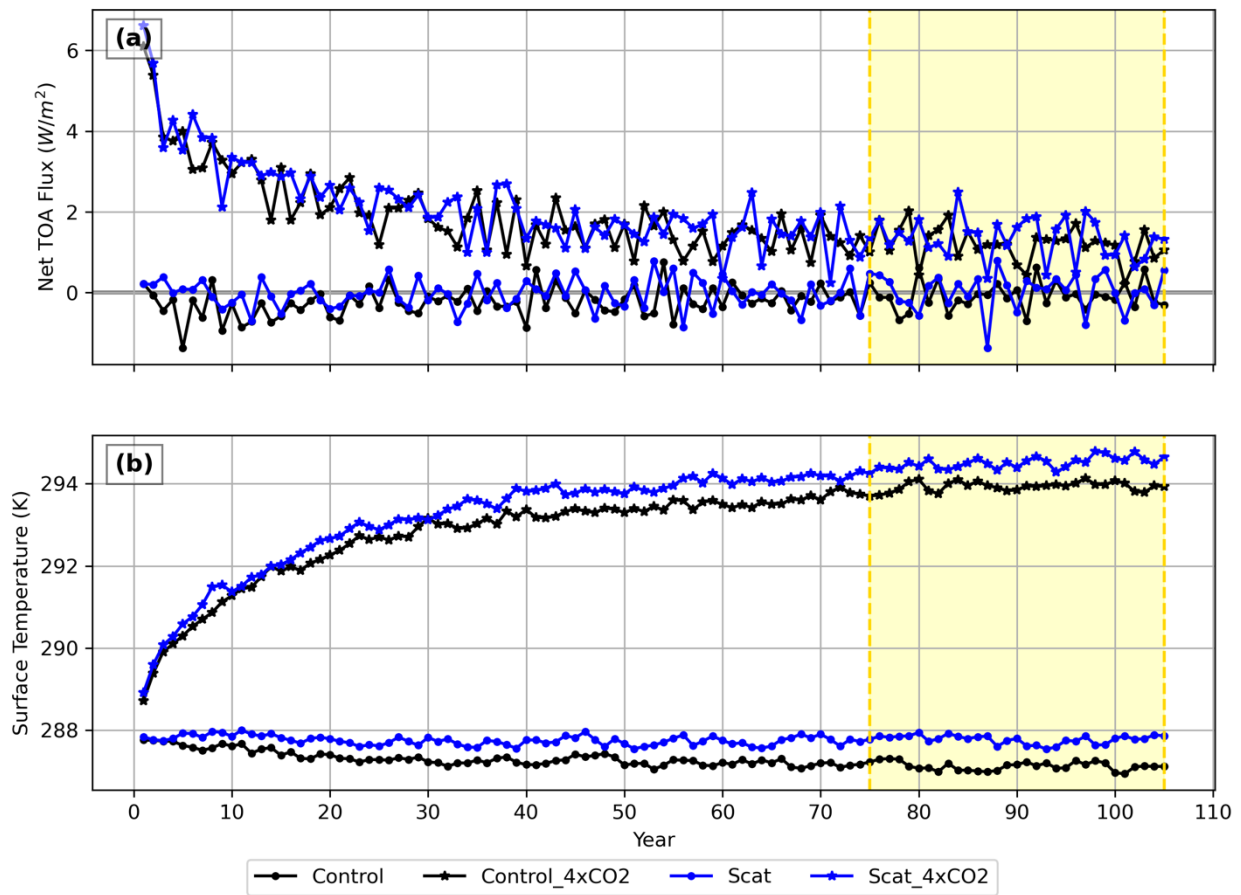
578 **Tables**

579 **Table 1.** Simulated global-mean net radiative flux change at the TOA (unit of W/m^2 , positive
 580 downward) due to the inclusion of cloud LW scattering. Wherever applicable, flux changes are
 581 separated into longwave and shortwave components. The instantaneous effect, fast response, and
 582 total response are shown, as well as their differences. Fast adjustment is decomposed into six terms
 583 using a radiative kernel. The sum of these individual terms is shown at the last row, which can be
 584 compared to the fast adjustment term at the fifth row.

	Longwave (W/m^2)	Shortwave (W/m^2)	Total (W/m^2)
Total Response	-0.606	0.717	0.111
Instantaneous Effect	1.127		1.127
Fast Response	0.670	0.023	0.692
Fast Adjustment (Fast Resp.– Instantaneous)	-0.457	0.023	-0.435
Slow Adjustment (Total Resp. – Fast Resp.)	-1.276	0.694	-0.581
<i>Contribution to the fast adjustment from different factors</i>			
Surface Temperature	-0.028		-0.028
Tropospheric Temperature	-0.260		-0.260
Stratospheric Temperature	0.013		0.013
Water Vapor	0.080	0.022	0.102
Surface Albedo		0.032	0.032
Cloud	-0.283	-0.021	-0.304
Sum of Individual Terms	-0.478	0.033	-0.445

585

586 **Figures**



587

588 **Figure 1.** Annual-mean time series of (a) global mean energy imbalance at the top of the

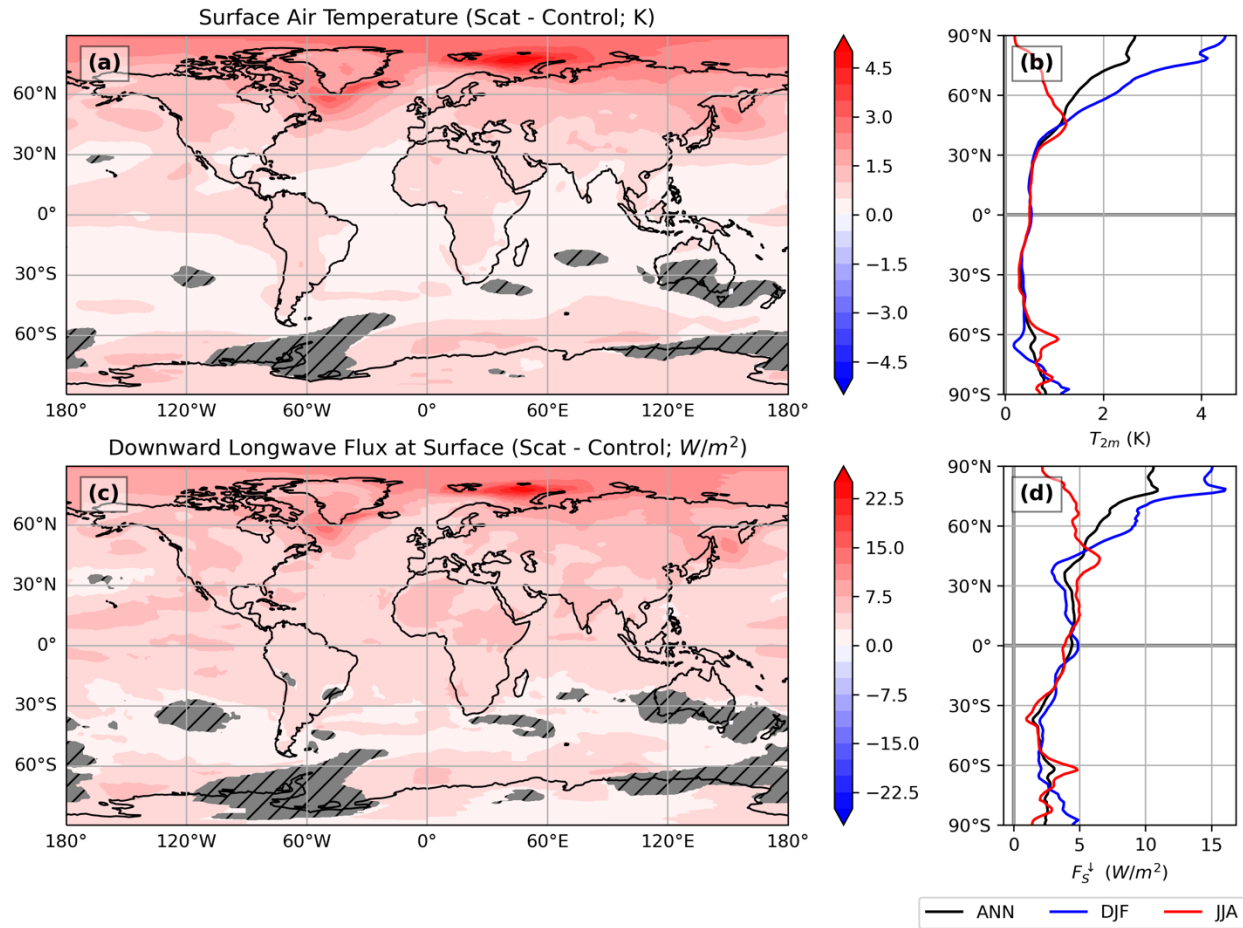
589 atmosphere (TOA), defined as net downward flux; and (b) global mean surface skin temperature.

590 The Scat and Control cases are shown in blue and black, respectively. The cases under preindustrial

591 control scenario are marked by dots, while the cases under 4×CO₂ scenario are marked by stars.

592 The yellow highlighted region indicates the time period we used in all climatological calculations.

593



594

595 **Figure 2.** Comparison of the surface climatology between the Scat case and the Control case. (a)

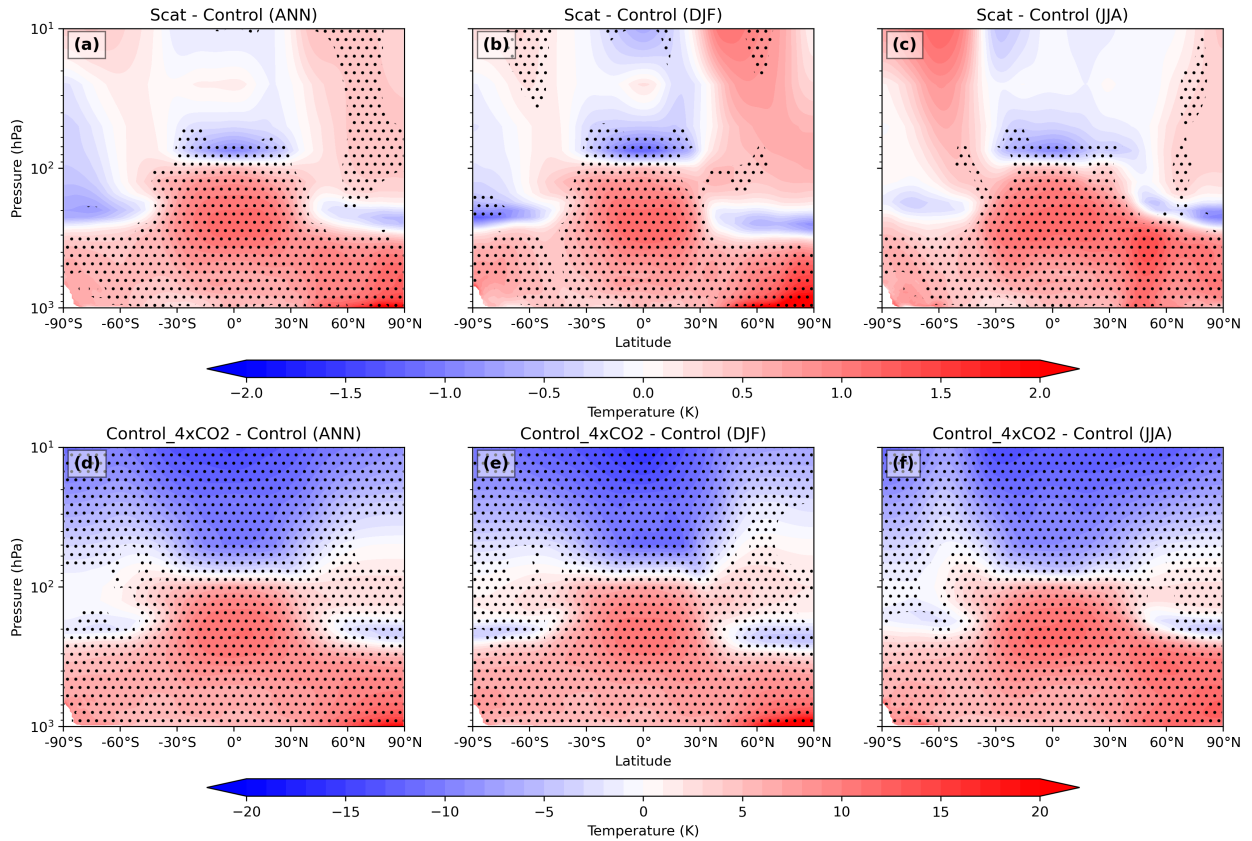
596 Annual-mean surface air temperature difference. (b) Zonal-mean surface air temperature

597 difference in annual mean (black), boreal summer season (JJA; red), and boreal winter season (DJF;

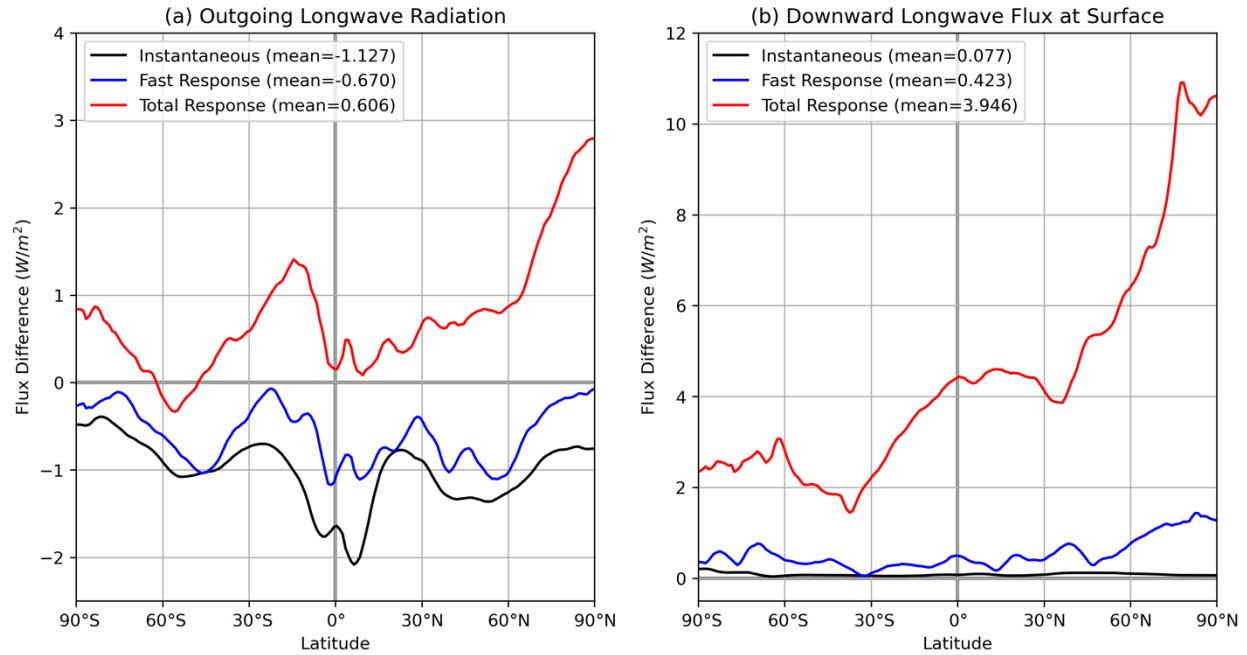
598 blue). (c,d) Same as (a,b) but for FLDS. Gray slat patches mask the region without statistically

599 significant changes (1% significance level).

600



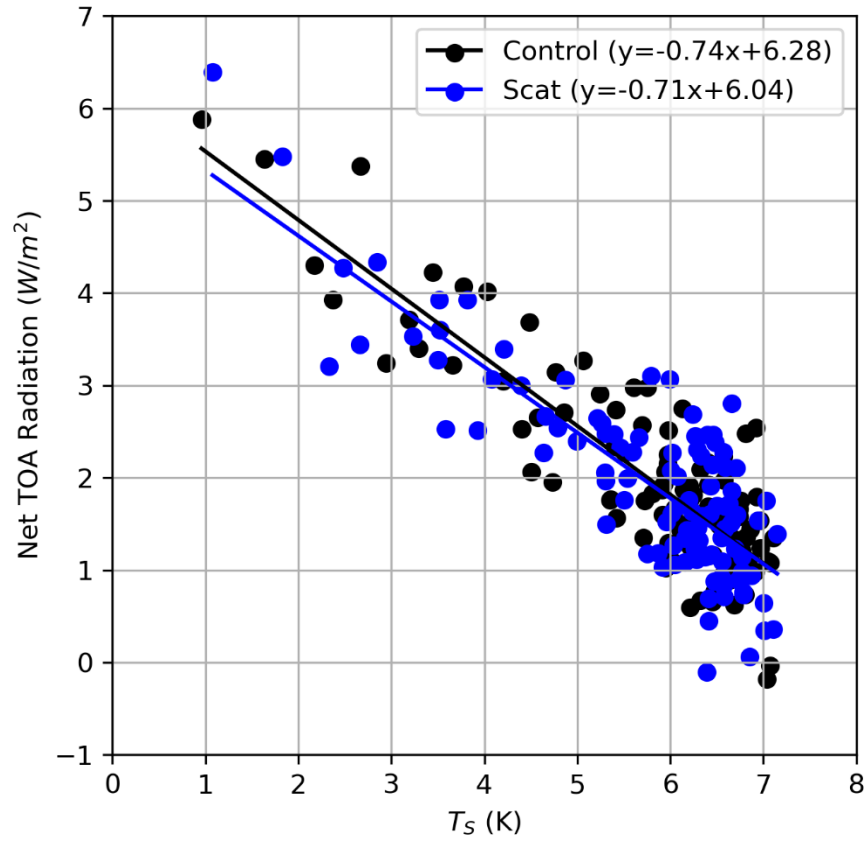
601
 602 **Figure 3.** (a) Annual- and zonal-mean differences in vertical temperature profile resulting from
 603 the cloud LW scattering effect; (b) the same zonal-mean difference but in boreal winter seasons
 604 (DJF); (c) the same zonal-mean difference but in boreal summer seasons (JJA); (d-f) the same as
 605 (a-c), but the contour shows the vertical temperature profile change due to abrupt 4×CO₂
 606 concentration. Black dots indicate statistically significant temperature change at 1% significance
 607 level.
 608



609

610 **Figure 4.** Zonal mean flux changes from instantaneous radiative effect (black), fast response (blue),
 611 and total response (red) caused by the inclusion of cloud LW scattering. (a) outgoing longwave
 612 radiation, where net upward is positive; (b) downward longwave flux at surface, where net
 613 downward is positive. The global average of each component is indicated in the legend.

614



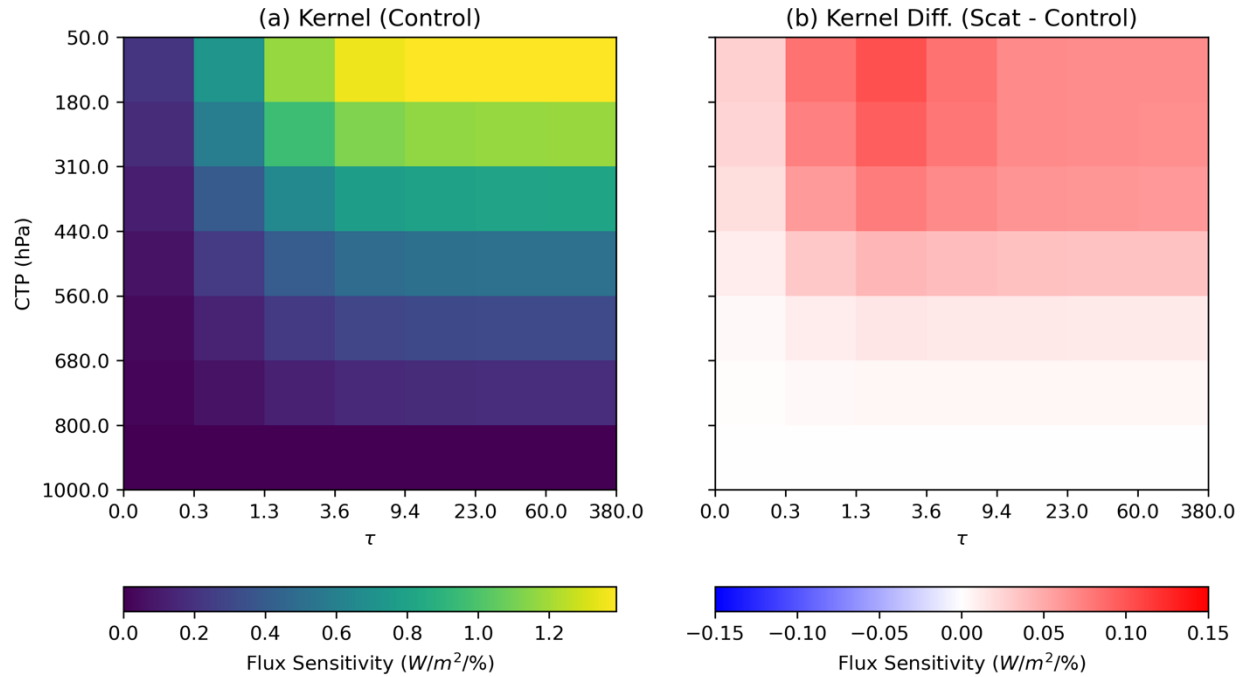
615

616 **Figure 5.** The relationship between the net TOA radiative flux and surface temperature (a.k.a., the

617 Gregory plot) in the Control case (black) and the Scat case (blue). The slope (i.e., climate

618 sensitivity) and the intercept (i.e., ERF) of each regression line are marked in the legend.

619



620

621 **Figure 6.** (a) Global and annual mean of the cloud LW radiative kernel we built based on the

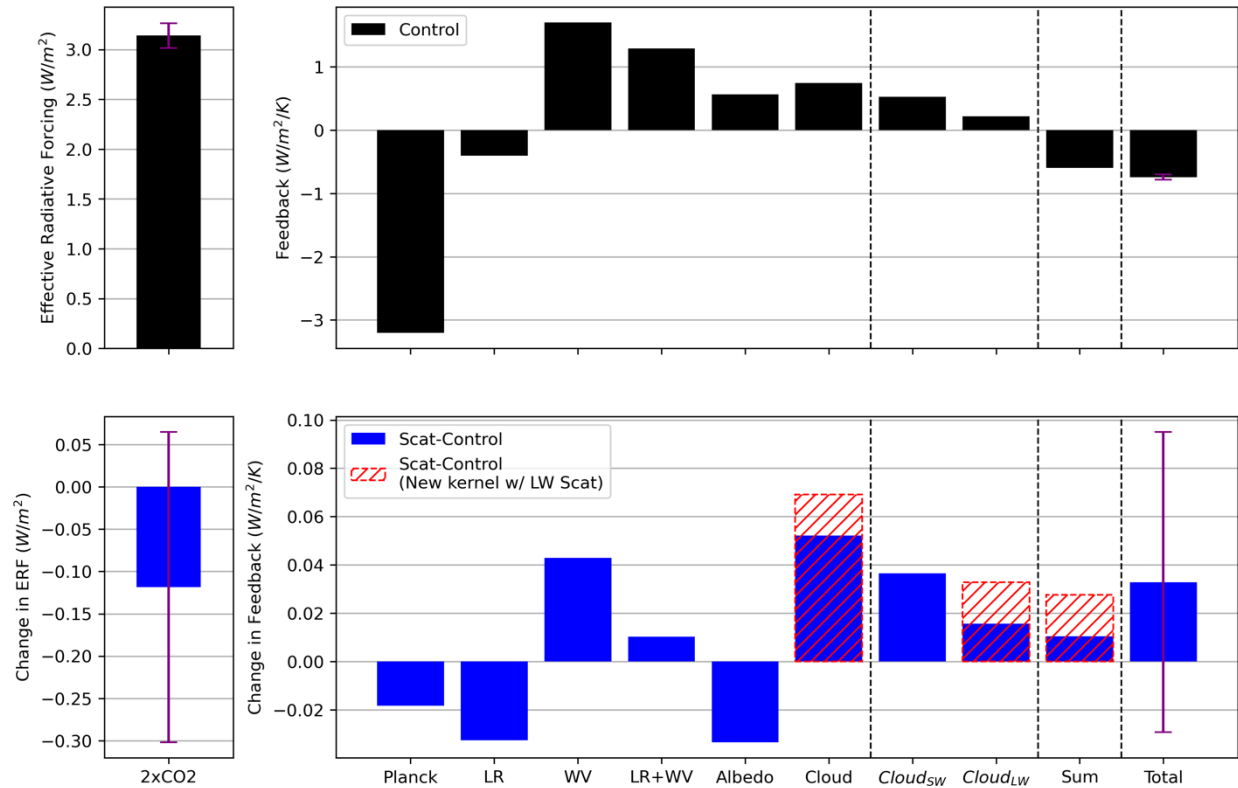
622 Control case. (b) The difference of the two kernels based on the Scat case and the Control case

623 (i.e., the correction term). τ is cloud optical thickness at a visible wavelength, and CTP is cloud

624 top pressure. Flux sensitivity is defined as the TOA flux change when we put a cloud with a specific

625 optical thickness at a specific pressure level (net downward is positive).

626



627

628 **Figure 7.** Effective radiative forcing and climate feedbacks estimated from the abrupt $4\times\text{CO}_2$

629 experiment with and without cloud LW scattering. The first row shows the absolute quantities in

630 the Control case, while the second row shows the differences between the Scat case and the Control

631 case. Values of $2\times\text{CO}_2$ ERF and total feedback are estimated from linear regression, while other

632 values are from radiative kernel analysis. The standard errors associated with the linear regression

633 in the Gregory plot (Fig. 5) are attached as purple stems on the corresponding terms. As usual,

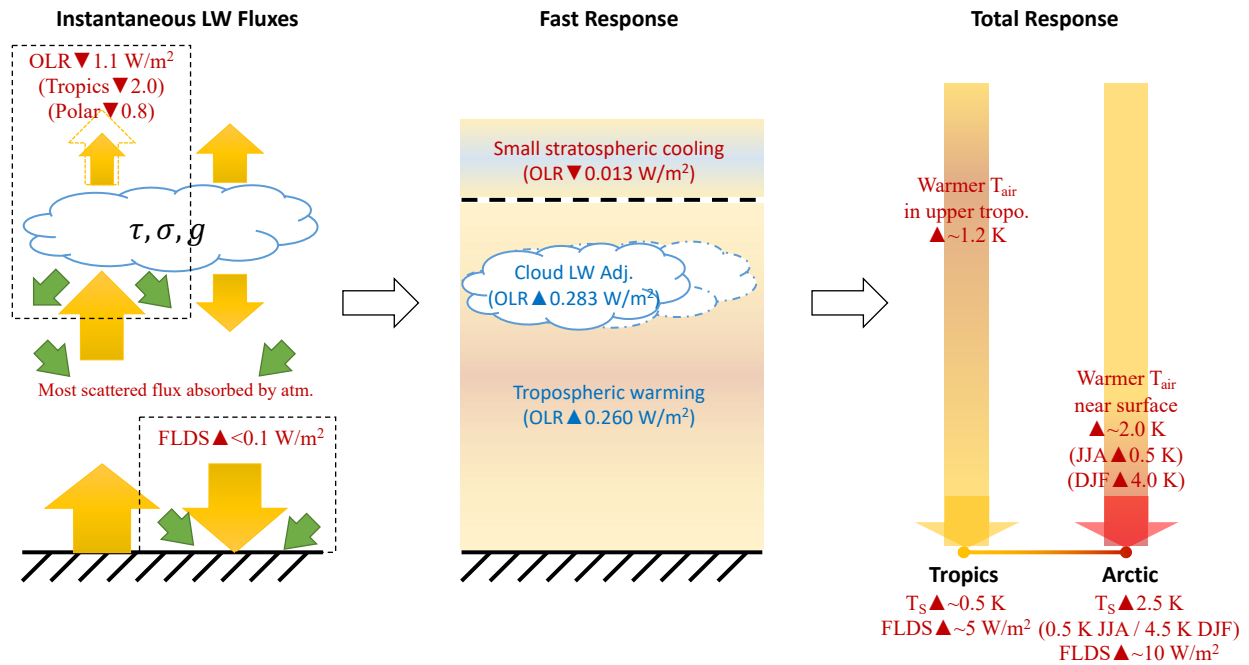
634 standard errors of the differences between Scat and Control are the Euclidean norm of the errors

635 in both cases (i.e., $\varepsilon_{diff} = (\varepsilon_{Control}^2 + \varepsilon_{Scat}^2)^{\frac{1}{2}}$). Red slat bars in the second row show the updated

636 values using the corrected cloud radiative kernel (i.e., when cloud LW scattering is considered).

637

638



639

640 **Figure 8.** Schematic summary of the instantaneous radiative effect (left), fast response (middle),
641 and total responses (right) due to the inclusion of cloud LW scattering in the E3SMv2. Only
642 prominent features are presented in the diagram. All red texts indicate a warming factor (i.e.,
643 increasing temperature and reducing OLR), while blue texts indicate a cooling factor (i.e.,
644 decreasing temperature and increasing OLR).

1 **Supplementary Materials for “A Refined Understanding of**
2 **the Ice Cloud Longwave Scattering Effects in Climate**
3 **Model”**

4
5 Chongxing Fan^{1*}, Yi-Hsuan Chen¹⁺, Xiuhong Chen¹, Wuyin Lin², Ping Yang³,
6 Xianglei Huang¹

7
8 ¹ Department of Climate and Space Sciences and Engineering, the University of Michigan, Ann Arbor,
9 Michigan, USA

10 ² Environmental & Climate Sciences Department, Brookhaven National Laboratory, New York State, USA

11 ³ Department of Atmospheric Sciences, Texas A&M University, Texas, USA

12
13 * Corresponding Author: Chongxing Fan (cxfan@umich.edu)

14 ⁺ Current affiliation: Research Center for Environmental Changes, Academia Sinica, Taipei, Taiwan

15
16
17
18 Submitted to *Journal of Advanced Modeling Earth Systems*

19 Original submission on November 5, 2022

20 Resubmission on May 7, 2023

21 Revision on August 23, 2023

22 **Contents of this file**

23 Figures S1 to S4.

24 **Introduction**

25 In this short introduction, we discuss the cloud field changes in fully-coupled simulations and
26 prescribed simulations due to cloud LW scattering.

27 Figure S2 shows the change in cloud ice content ratio due to cloud LW scattering. We define
28 the cloud ice content ratio as the ratio of in-cloud ice mixing ratio (r_{ice}) and in-cloud total water
29 mixing ratio ($r_{total} = r_{ice} + r_{liquid}$). In the fully coupled simulations (first row), we can see a
30 general cloud ice-to-liquid transition all over the globe, but there is a prominent ice-to-liquid
31 transition at approximately 600 hPa in the tropics. The ice content ratio decrease can be up to 20%.
32 We cannot see such a strong effect in the prescribed runs (second row), suggesting that this cloud
33 phase transition is mostly caused by the slow adjustment. Such cloud phase transition is also
34 observed in the response to the 4xCO₂ experiment.

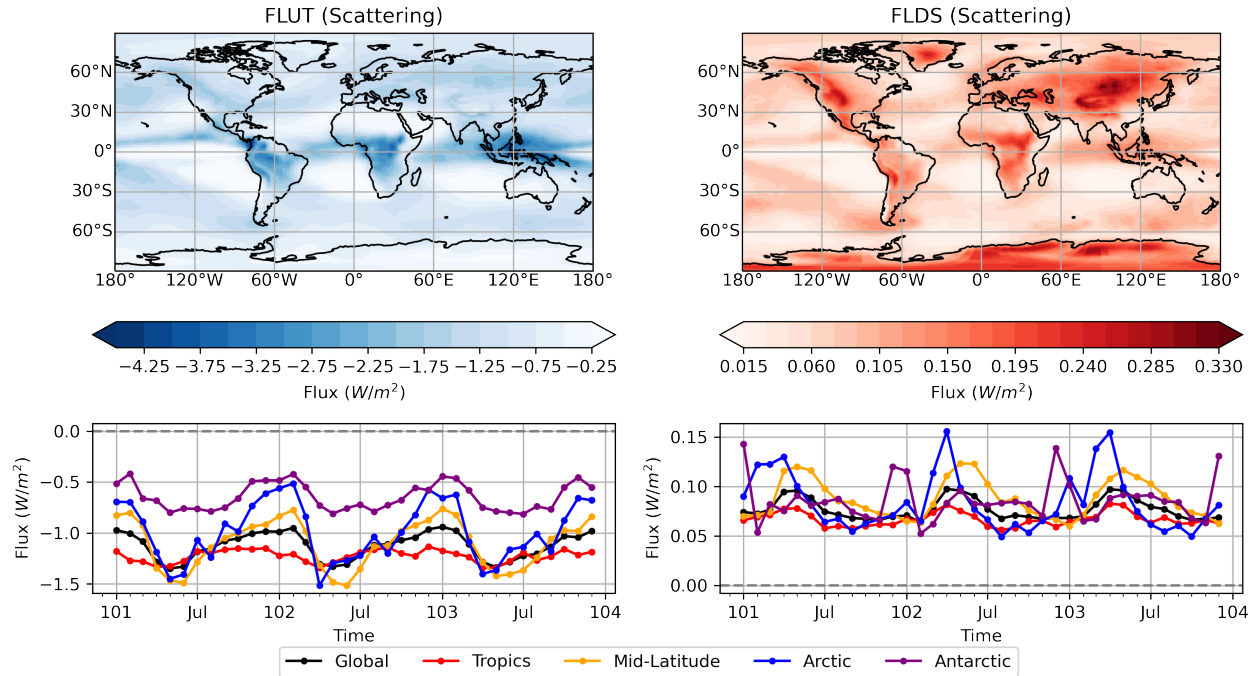
35 Figure S3 shows the change in vertically-resolved cloud fraction in the deep tropics (20°S ~
36 20°N) due to cloud LW scattering. In general, we see a strong cloud fraction reduction at 200 hPa
37 in all cases, and a relatively smaller cloud fraction increase at ~150 hPa. These patterns of high-
38 cloud change are also seen in the 4xCO₂ experiments with a different magnitude (lowest row), i.e.,
39 elevated deep convective cloud and reduced anvil cloud coverage. Again, they are also the result
40 of slow adjustments when the cloud LW scattering is included in the model.

41 Figure S4 shows the low cloud fraction change due to cloud LW scattering. We follow the
42 definition used in climate models, which categorizes clouds with a cloud top pressure > 700 hPa
43 as low clouds. An increase of low cloud fraction by up to ~0.06 is seen over the southeastern
44 tropical Pacific, southern subtropical Atlantic, and Indian Ocean. Those regions are known for the

45 frequent occurrence of stratiform low clouds. These patterns of low cloud increases are similar to
46 the counterpart pattern in the response to the increase of CO₂ predicted by the E3SMv2 model, but
47 the magnitude of change and statistical significance of such changes are notably different.

48

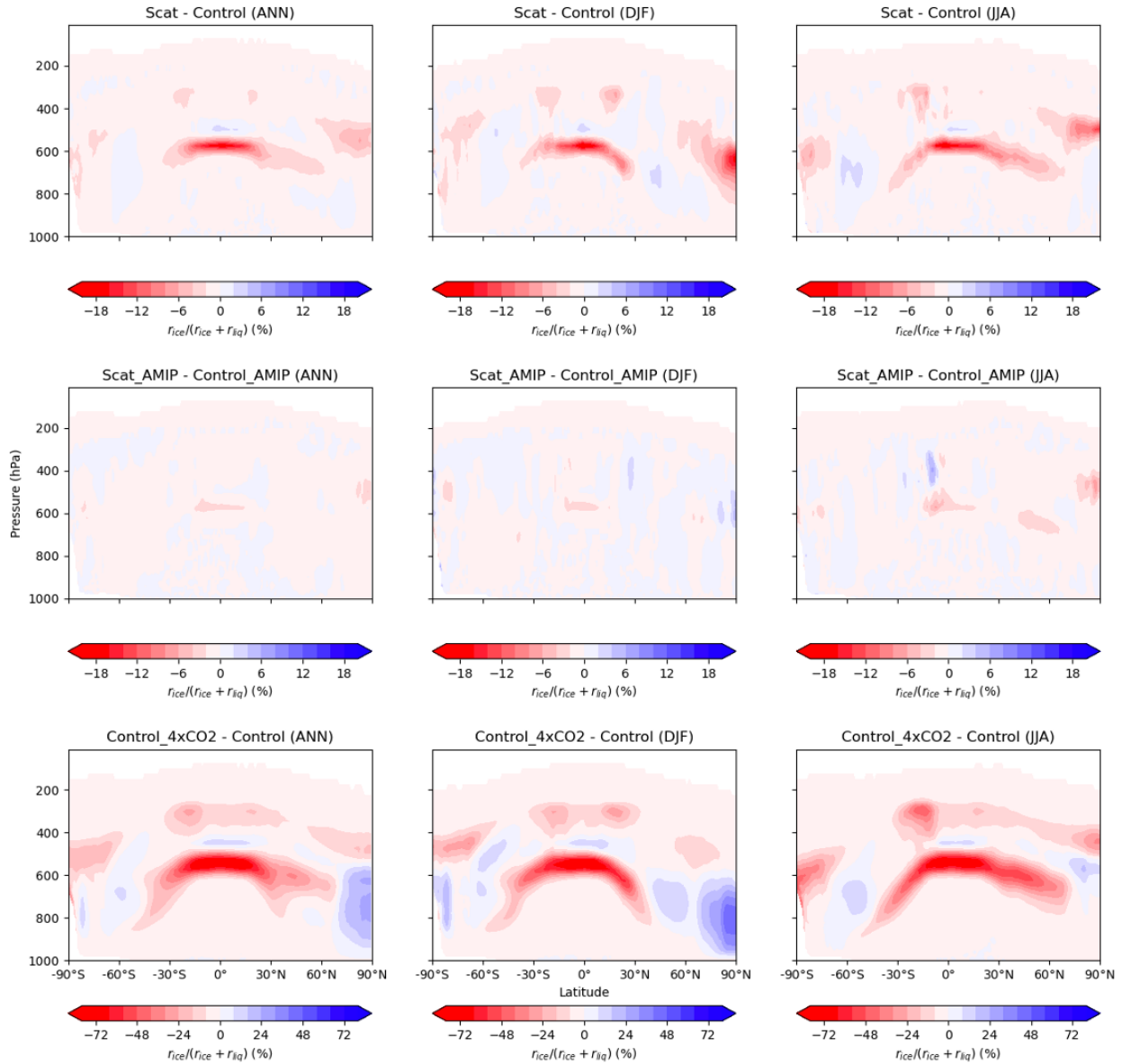
49



50

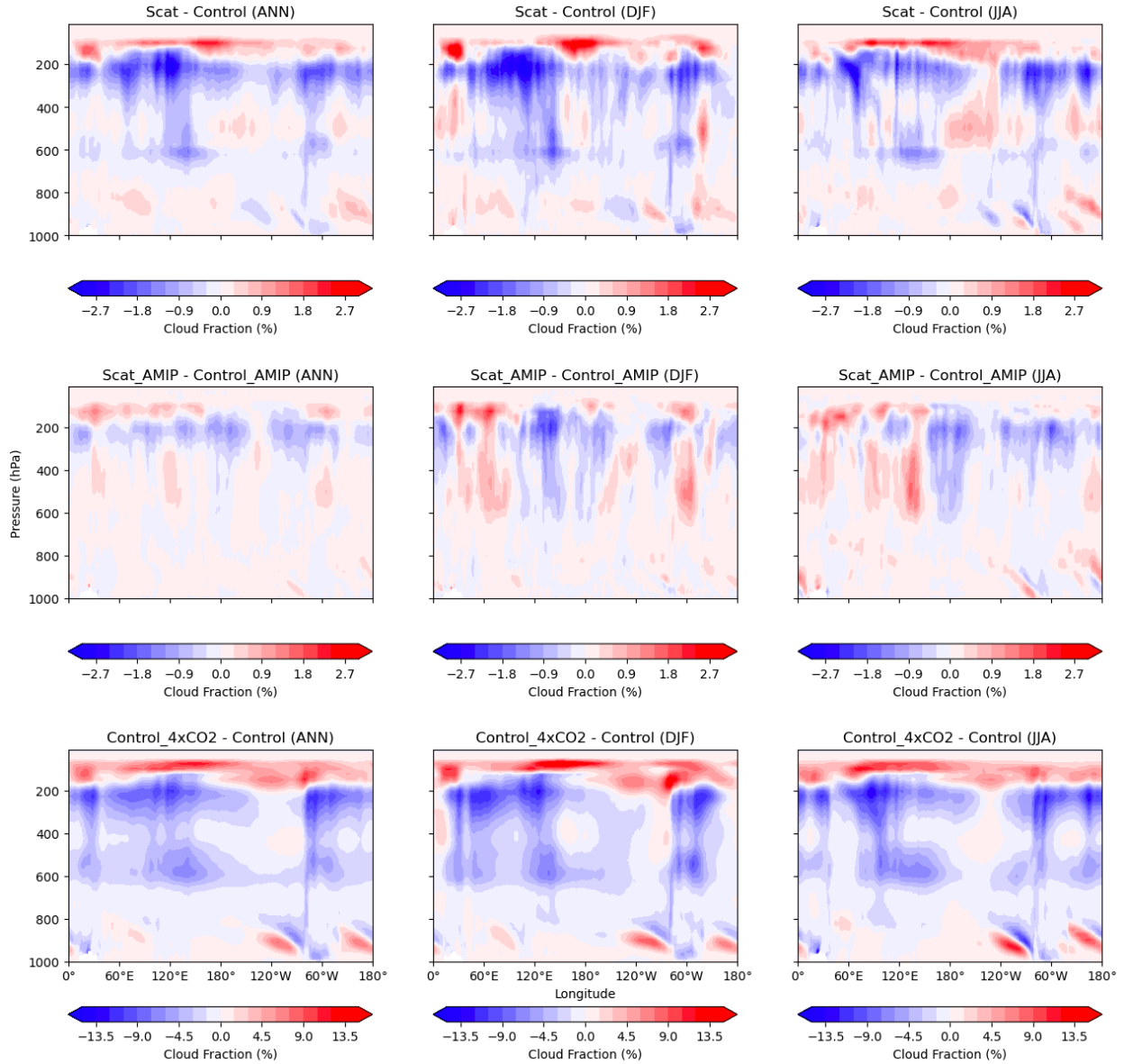
51 **Figure S1.** Changes in the upward longwave radiative flux at the top of the atmosphere (FLUT;
 52 left column) and the downward longwave radiative flux at the surface (FLDS; right column) due
 53 to the direct LW scattering effect. The top row shows the spatial distribution of the three-year
 54 mean change, and the bottom row shows the time series of global and regional mean changes in
 55 the first three years. Note that the global and regional mean changes have apparent seasonal cycles,
 56 but the annually averaged changes vary little from year to year. Each tick on the x-axis of the
 57 bottom panels represents a month starting from January of the year 101.

58



59

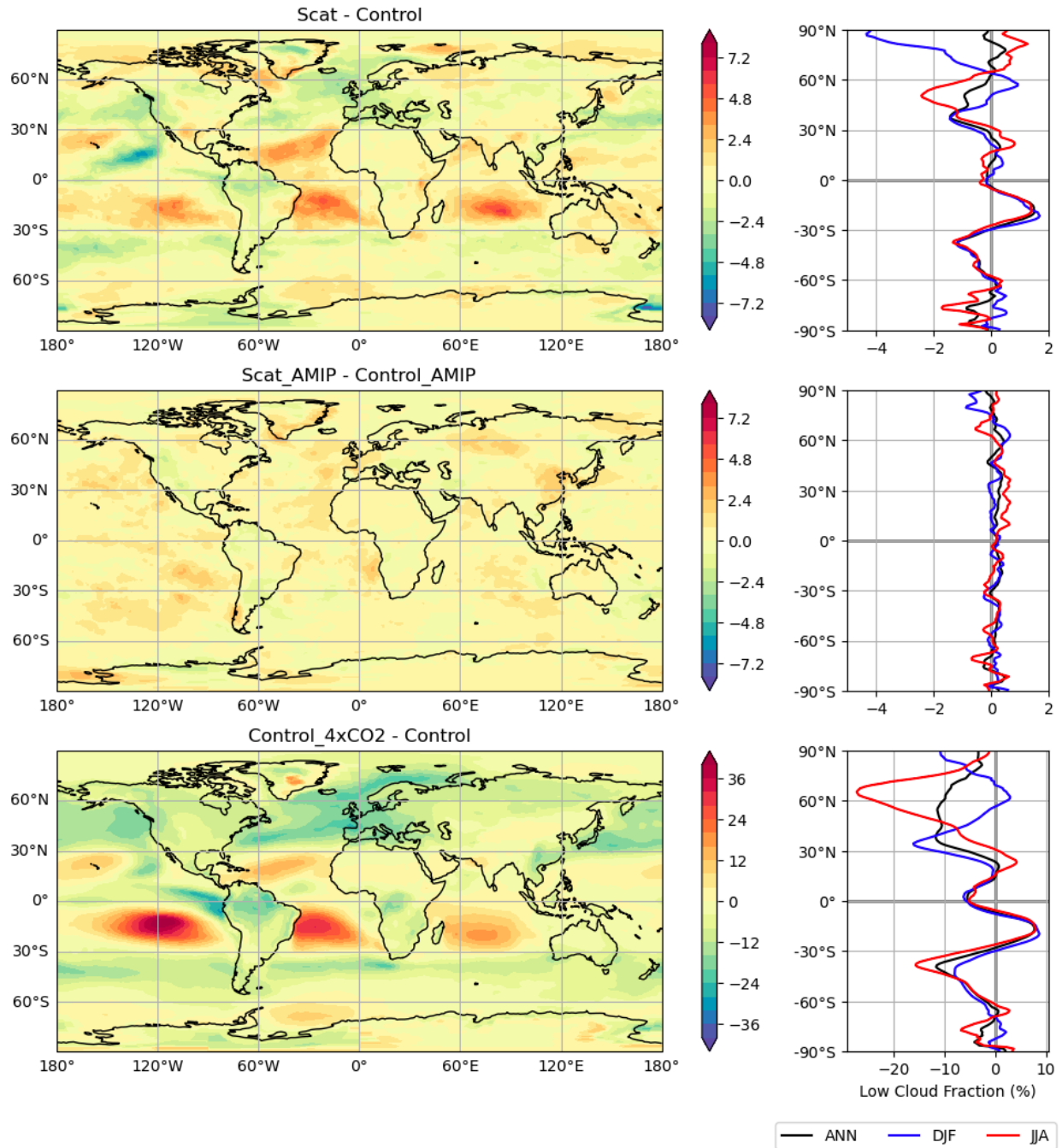
60 **Figure S2.** Zonal-mean cloud ice content ratio (i.e., the ratio of in-cloud ice mixing ratio and in-
 61 cloud total water mixing ratio) difference. Negative value (red) means ice-to-liquid transition,
 62 while positive value (blue) means the opposite. The first two rows are the differences resulting
 63 from cloud LW scattering effect in the fully-coupled run and the prescribed run, respectively. The
 64 third row shows the difference resulted from 4xCO₂ concentration. The first column shows the
 65 annual-mean difference, the second column shows the mean difference in boreal winters, and the
 66 third column shows the mean difference in boreal summers.



67

68 **Figure S3.** Similar to Figure S2, but this one shows the latitudinal-mean profile difference of the
 69 cloud fraction in the deep tropics (20°S ~ 20°N). Negative value (blue) indicates less cloud
 70 coverage, while positive value (red) indicates the opposite.

71



72

73 **Figure S4.** Low cloud fraction change. The first two rows are the differences resulting from cloud
 74 LW scattering effect in the fully-coupled run and the prescribed run, respectively. The third row
 75 shows the difference resulted from 4xCO₂ concentration. The first column shows the contour map

76 of the annual-mean difference, while the second column shows the zonal-mean difference in all
77 seasons (black), boreal winters (blue), and boreal summers (red).

78